NBI Beam Ion Distributions in the Presence of Magnetic Islands in Helical Plasmas*)

Hiroyuki YAMAGUCHI and Sadayoshi MURAKAMI
Department of Nuclear Engineering, Kyoto University, Kyoto 615-8530, Japan
(Received 30 November 2015 / Accepted 18 April 2016)

Neutral beam injection (NBI) heating simulations of Large Helical Device (LHD) plasma in the presence of magnetic islands are performed using a drift kinetic equation solver, GNET. A magnetic perturbation that causes a magnetic island with poloidal and toroidal mode numbers $(m, n) = (1, 1)$ is considered. It is found that the spatial distribution of beam ions for counter-tangential NBI is significantly modified near the magnetic island, exhibiting a strong dependency on the mode phase of the island. The changes in the velocity space distribution and orbits of the transition particles imply an enhancement in the ripple transport of beam ions near the magnetic island.
© *2016 The Japan Society of Plasma Science and Nuclear Fusion Research*

Keywords: Large Helical Device, magnetic island, energetic particle, simulation, Monte Carlo, GNET

DOI: 10.1585/pfr.11.2403094

1. Introduction

The existence of closed and nested magnetic surfaces in a large fraction of plasma volume is an essential requirement for good plasma confinement in toroidal devices. However, resonant radial magnetic perturbations due to plasma instabilities or external error fields can produce magnetic islands, which tear the original magnetic surface and enhance the radial transport of heat and particles. On the contrary, plasma performance can be improved by externally imposing resonant magnetic perturbation (RMP) and producing magnetic islands in the plasma. For example, it is well-known that the edge localized mode can be stabilized by imposing RMPs in tokamaks. A number of experimental and theoretical studies on fast ion confinement in tokamaks have been done in the presence of magnetic islands associated with RMP. The RMP experiment has been also done in the Large Helical Device (LHD), which is equipped with superconducting helical coils [1–3]. A detailed study of fast ion behavior in the LHD with magnetic islands, as done in tokamaks, is equally important to understand the RMP effect on fast ion confinement in helical plasmas.

In this study, we investigate fast ion distribution in helical plasma in the presence of magnetic islands with numerical simulations using the GNET code [4]. We consider the beam ions generated by neutral beam injection (NBI) heating in the LHD, and investigate the effect of magnetic islands with mode numbers relevant to the RMP experiment at LHD.

This paper is organized as follows. In the next section, we briefly explain the simulation model used in this study. In Section 3, the simulation results are shown focusing on the spatial and velocity space distribution and the loss fraction of the NBI beam ions. Finally, we summarize this study in the last section.

2. Simulation Model

In helical systems, the NBI beam ions perform complex guiding-center motion in a three-dimensional magnetic configuration. In this study, using the GNET code based on the Monte Carlo method, we solve a drift kinetic equation for NB-born fast beam ions in five-dimensional phase space. The drift kinetic equation is

$$\frac{\partial f_\mathrm{b}}{\partial t} + (\mathbf{v}_\parallel + \mathbf{v}_\mathrm{D}) \cdot \nabla f_\mathrm{b} + \dot{\mathbf{v}} \cdot \nabla_v f_\mathrm{b} = C(f_\mathrm{b}) + L(f_\mathrm{b}) + S_\mathrm{NBI}, \quad (1)$$

where f_b is the beam ion distribution function, $\mathbf{v}_\parallel$ is the velocity parallel to the field line, $\mathbf{v}_\mathrm{D}$ is the drift velocity, C is the linear Coulomb collision operator, L is the particle loss term, and S_NBI is the particle source term of the NBI evaluated by the HFREYA code, which is a part of the FIT3D code [5].

The complex guiding-center motion of beam ions are taken into account by solving the Hamiltonian equations for the test particle's guiding-center motion in Boozer coordinates [6]. We assume that the magnetic field is expressed as a sum of the equilibrium field, $\mathbf{B}_0$, and a perturbation, $\delta\mathbf{B}$

$$\mathbf{B} = \mathbf{B}_0 + \delta\mathbf{B}. \quad (2)$$

The spectrum of the equilibrium magnetic field in Boozer coordinates is constructed from the equilibrium by VMEC. The perturbation part is given by

$$\delta\mathbf{B} = \nabla \times (\alpha\mathbf{B}_0), \quad (3)$$

author's e-mail: yamaguchi@p-grp.nucleng.kyoto-u.ac.jp
*) This article is based on the presentation at the 25th International Toki Conference (ITC25).

© 2016 The Japan Society of Plasma Science and Nuclear Fusion Research

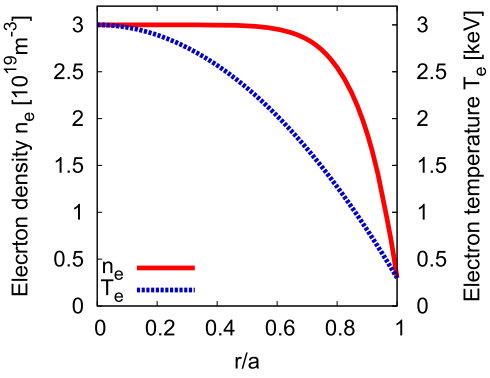

Fig. 1 Radial profiles of the electron density and electron temperature used in the simulation.

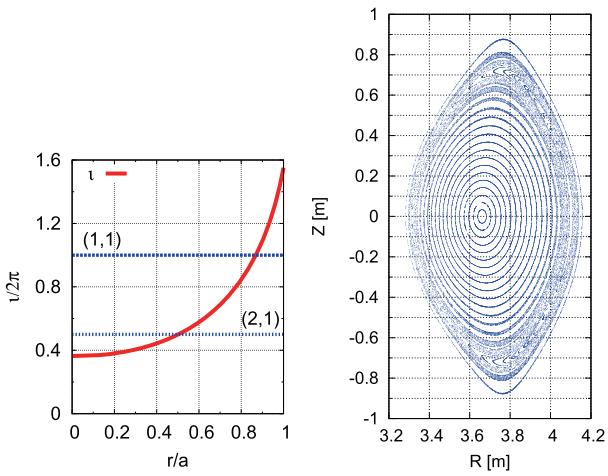

Fig. 2 Radial profile of the rotational transform, ι, (left) and a Poincaré plot of the field lines of the LHD configuration with a $(m, n) = (1, 1)$ magnetic island (right).

which produces magnetic islands at the resonant rational surfaces. The Hamiltonian equations for the guiding-center motion with this type of magnetic perturbation have been derived [7]. In this study, we implemented these equations in GNET. We assumed a static perturbation with

$$\alpha = \alpha_{m,n}(r)\cos(m\theta - n\zeta + \delta), \tag{4}$$

where r is the minor radius, θ and ζ are the poloidal and toroidal angle coordinates, respectively, m and n are the poloidal and toroidal mode numbers of the perturbation, respectively, and δ is a parameter to control the phase. The radial profile of the perturbation is assumed to be

$$\alpha_{m,n} = \alpha_0^{m,n}\left(\frac{r}{r_0}\right)^k\left(\frac{1-r}{1-r_0}\right)^p, \tag{5}$$

where r_0 is the peak position of the mode, k is an integer to set the profile shape, and $p = k(1/r_0 - 1)$. In this study, we fixed k to be 8.

The pitch-angle and energy scatterings due to Coulomb collisions with bulk plasma, as well as the energy slowing down, are considered in C. The test particles are followed until they are lost from the outer-most flux surface or their kinetic energy reaches the thermal energy. In this study, the thermal energy is defined as $3T_i/2$, where T_i is the ion temperature at the instantaneous location of the test particle. The electron density, n_e, electron temperature, T_e, and ion temperature are assumed to be

$$n_e = 3 \times \left[1 - 0.9(r/a)^8\right]\ [10^{19}\mathrm{m}^{-3}], \tag{6}$$

$$T_e = 3 \times \left[1 - 0.9(r/a)^2\right]\ [\mathrm{keV}], \tag{7}$$

$$T_i = T_e, \tag{8}$$

where r/a is the normalized minor radius. The radial profiles of n_e and T_e are shown in Fig. 1.

We assume an equilibrium magnetic field of LHD with $R_{ax} = 3.6$ m and $B_0 = -2.85$ T, where R_{ax} and B_0 are the position of the magnetic axis and the field strength at the magnetic axis, respectively. In this study, we consider the $(m, n) = (1, 1)$ mode with $\alpha_0^{1,1}/a = 4 \times 10^{-4}$, where a is the minor radius at the outer-most flux surface. Figure 2 shows the radial profile of the rotational transform for this equilibrium. Figure 2 also shows a Poincaré plot of the magnetic field lines in the presence of this magnetic perturbation. We can see a magnetic island appearing at the resonant surface.

We studied the counter-tangential NBI (ctr-NBI) of the LHD. The beam energy was set to 180 keV.

3. Simulation Result

Figure 3 shows the radial distributions of the beam ion density and the relative differences caused by the presence of a magnetic island. The center-peaked profiles inside $r/a < 0.6$ were nearly unaffected by the magnetic island. When the magnetic island was present, the beam ion density was changed by approximately 40% near the resonant surface. In the case with $\delta = 0$, the beam ion density increased at the resonant surface and decreased in its neighboring areas. This pattern of variation in the beam ion density was reversed when $\delta = \pi$; the beam ion density decreased at the resonant surface and increased in its neighboring areas. Figure 4 shows the contour plots of the beam ion pressure on a poloidal cross-section at $\zeta = 0$ for the cases without magnetic perturbation (top) and with a magnetic island with $\delta = 0$ (middle) and $\delta = \pi$ (bottom). The unit in Fig. 4 is arbitrary. In the case of $\delta = 0$, the beam ion pressure is strongly localized and an island structure is formed at the resonant surface. Whereas, in the case of $\delta = \pi$, we can see a vacant hole in the beam ion pressure at the resonant surface.

Figure 5 shows a contour plot of the beam ion distribution function in velocity space averaged over the resonant surface in the absence of a magnetic island. Figure 5 also shows the change in the distribution function caused by the magnetic island with $\delta = 0$ and $\delta = \pi$. The increased part is colored in red and the decreased part is colored in blue.

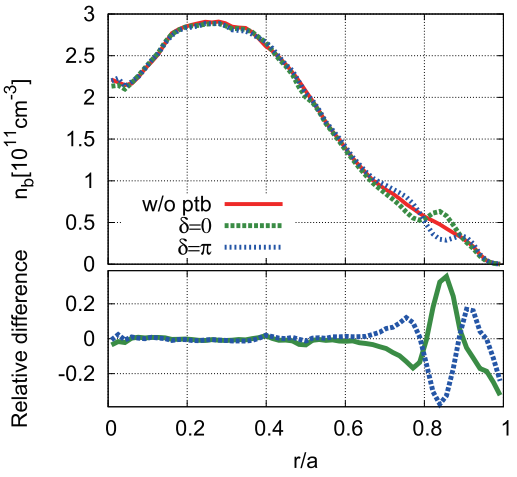

Fig. 3 Radial profiles of the beam ion density, n_b, and the relative difference from the case without a magnetic perturbation (ptb).

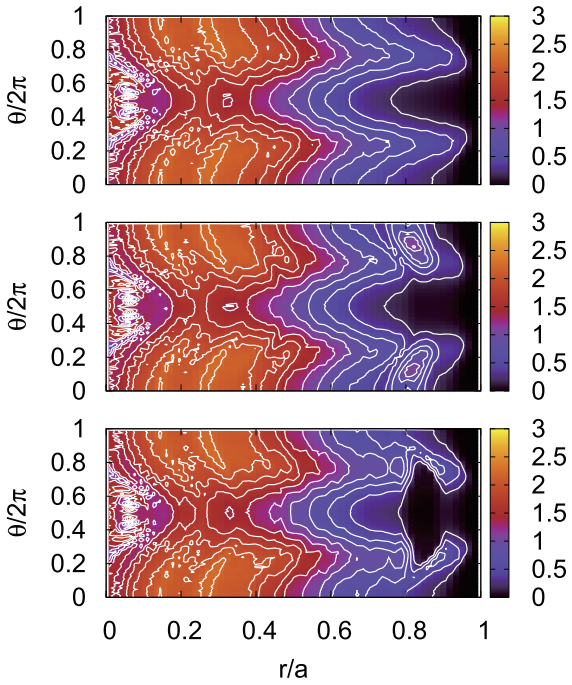

Fig. 4 Contour plots of the beam pressure of ctr-NBI on a poloidal cross-section at $\zeta = 0$ without magnetic perturbation (top) and with a $(m, n) = (1, 1)$ magnetic island with a phase of $\delta = 0$ (middle) and $\delta = \pi$ (bottom).

The units are arbitrary. The same graphs for an outer surface at $r/a = 0.92$ are shown in Fig. 6. The distribution function at the resonant surface in the absence of a magnetic island shows slowing down of the counter-passing beams and the subsequent pitch-angle scatterings, with the former dominated by electrons and the latter by the bulk ions. The counter-passing beams increase in the case with $\delta = 0$ and decrease in the case with $\delta = \pi$. On the outer surface at $r/a = 0.92$, these variations are reversed for each phase of the magnetic island.

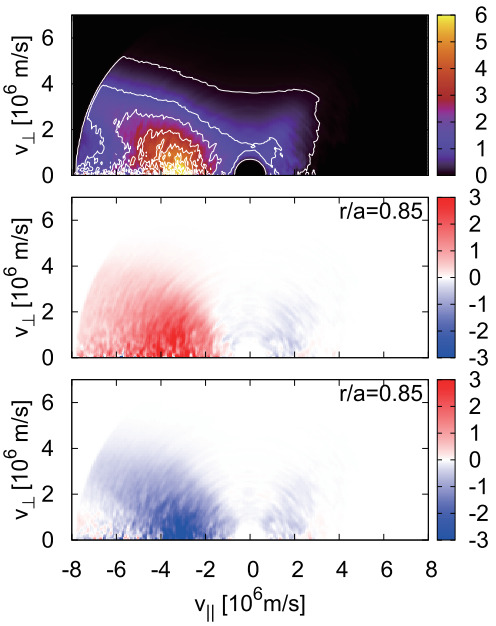

Fig. 5 Velocity-space distribution of the beam ions for ctr-NBI at $r/a = 0.85$ (top), and the differences caused by the present of a $(m, n) = (1, 1)$ magnetic island with $\delta = 0$ (middle) and $\delta = \pi$ (bottom).

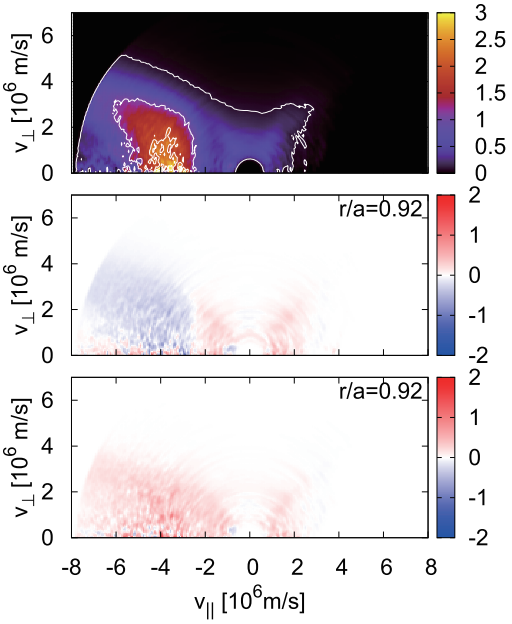

Fig. 6 Velocity-space distribution of the beam ions for ctr-NBI at $r/a = 0.92$ (top), and the differences caused by the present of a $(m, n) = (1, 1)$ magnetic island with $\delta = 0$ (middle) and $\delta = \pi$ (bottom).

These simulation results indicate that the beam ions of ctr-NBI are well confined in or nearly barred from the magnetic island during their slowing down, depending on the phase of the magnetic island. Most of the beam ions produced by ctr-NBI are counter-passing particles. These passing particles move, to the first approximation, along

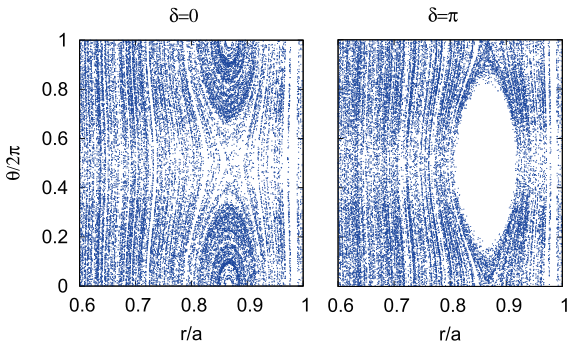

Fig. 7 Poincaré plots of magnetic field lines staring from the birth points of ctr-NBI in the presence of a magnetic island with phase $\delta = 0$ (left) and $\delta = \pi$ (right).

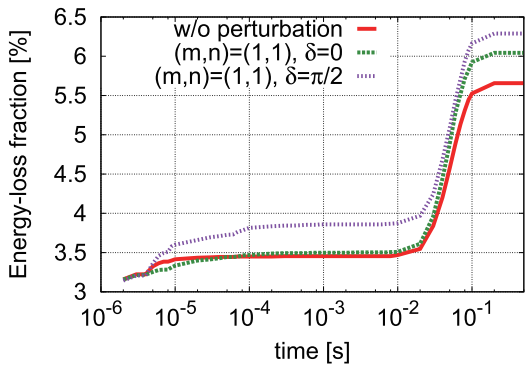

Fig. 8 Time evolution of the loss fraction of the beam ion energy.

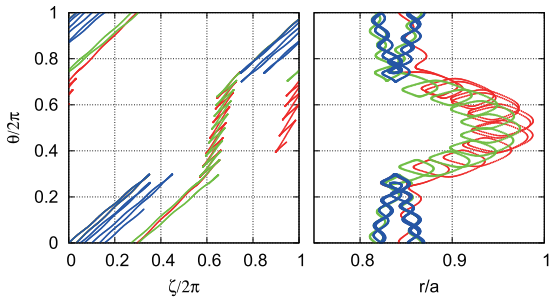

Fig. 9 Orbits of a trapped particle starting from $r/a = 0.85$, $\theta = \zeta = 0$ projected on θ-ζ plane (left) and on r/a-θ plane (right).

the field lines on which they originate. Therefore, the distribution of the birth points of the beam ions inside/outside the magnetic island greatly affects the beam ion distribution of ctr-NBI. To demonstrate this, we drew a Poincaré plot of the magnetic field lines traced starting from the birth points of ctr-NBI in Fig. 7. This figure directly illustrates the location of the birth points inside and outside the magnetic island. We can see that the beam ions only originate at the periphery of the magnetic island in the case with $\delta = \pi$, in contrast to the case with $\delta = 0$ where a number of beam ions originate in the core of the magnetic island.

The dependence on the phase of the island is also reflected in the time evolution of the energy-loss fraction, which is shown in Fig. 8. We can see two distinct types of beam ion loss, i.e., a pronpt loss of energetic beams occurring at $t < 10^{-4}$ s and a diffusive loss of partially slowed-down beams occurring at $t > 10^{-2}$ s. We can see that, in both phase cases, the diffusive loss of the beam ions is increased in the presence of a magnetic island. A clear difference can be seen in the prompt losses, which account for approximately 60% of the total losses. In the case with $\delta = \pi$, the prompt losses are increased. This indicates that the orbits of the passing particles that are barred from the island core wander greatly in the radial direction enhancing the prompt losses.

In contrast to the counter-passing beam ions, the beam ions with co-parallel velocities decrease on the resonant surface as can be seen in Fig. 5 regardless of the phase δ. We can also see an increase in the symmetric distribution on the outer surface. These beam ions with relatively small pitch, which is expressed by the ratio of the parallel velocity to the total, $\lambda = v_{\parallel}/v$, may be transition particles, whose orbits transit between passing, toroidally trapped, and helically trapped orbits depending on their location. To understand the behavior of trapped particles in the presence of a magnetic island, we followed the collisionless orbits of a typical trapped particle (50 keV, $\lambda = 0.4$) starting from $\theta = \zeta = 0$ on the resonant surface in Fig. 9. This starting point was located near the O-point ($\delta = 0$) and the X-point ($\delta = \pi$) of the magnetic island. In the absence of the magnetic island, this particle behaved as a toroidally trapped particle (blue line). When the magnetic island with $\delta = 0$ was present, this particle was trapped in a helical ripple after several toroidal bounces (green line), as seen in Fig. 9. When $\delta = \pi$, the orbit was similar to that of $\delta = 0$; however, there was another transition to a ripple trapped orbit (red line). These results indicate that the transition to the trapped orbits may be enhanced near the magnetic island. The change in the transition particle distribution in velocity space may be caused by an increase in the ripple transport in the presence of a magnetic island. It is still not clear whether the increase in the diffusive loss in the presence of a magnetic island is due to the enlarged orbit width of the passing particles or the enhancement of the transition of the trapped orbits.

4. Summary

We performed NBI heating simulations in the presence of static magnetic islands, assuming an LHD configuration. A magnetic island with poloidal and toroidal mode numbers $(m, n) = (1, 1)$, which was produced in the LHD experiment, was assumed. The drift kinetic equation was solved using the GNET code for the beam ion distribution function in 5-D phase space, taking into account the perturbed magnetic field. We performed the simulation for ctr-NBI.

In the presence of a magnetic island, the beam ion density of ctr-NBI was strongly modified near the resonant surface compared to that without a magnetic island. A localized beam ion pressure was formed in the presence of a magnetic island with a specific phase. By changing the phase of the magnetic island by π, it was found that the beam ions originating from within the magnetic island were significantly decreased and a vacant hole region appeared in the beam pressure distribution. In this case, the prompt loss of beam energy increased. The diffusive loss, by contrast, increased regardless of the mode phase. The changes in the velocity space distribution and the orbit of transition particles implied an enhancement in the ripple transport in the presence of a magnetic island near the resonant surface.

In the future, we will perform simulations of co-tangential NBI and perpendicular NBI in the presence of magnetic islands including the $(m, n) = (2, 1)$ mode, which is another island produced in the LHD experiment. Furthermore, we will evaluate the beam density distribution in the presence of magnetic islands and structure of the electrostatic potentials caused by the localized beam ion density.

Acknowledgements

This work was supported by JSPS KAKENHI Grant Number 26420851, 15J08296.

[1] T. Kobuchi *et al.*, J. Phys. Conf. Series **123**, 012021 (2008).
[2] Y. Narushima *et al.*, Plasma Fusion Res. **8**, 1402058 (2013).
[3] Y. Narushima *et al.*, Nucl. Fusion **55**, 073004 (2015).
[4] S. Murakami *et al.*, Fusion Sci. Technol. **46**, 214 (2004).
[5] S. Murakami *et al.* Fusion Technol. **27**, Suppl. S, 256 (1995).
[6] A.H. Boozer and G. Kuo-Petravic, Phys. Fluids **24**, 851 (1981).
[7] R.B. White and M.S. Chance, Phys. Fluids **27**, 2455 (1984).